Taking into Account Atmospheric Uncertainty Improves Sequential Assimilation of SMOS Sea Ice Thickness Data in an Ice–Ocean Model

Qinghua Yang

*Key Laboratory of Research on Marine Hazards Forecasting, National Marine Environmental Forecasting Center, Beijing,
China, and Alfred Wegener Institute, Helmholtz Centre for Polar and Marine Research, Bremerhaven, Germany*

Martin Losch and Svetlana N. Losa

Alfred Wegener Institute, Helmholtz Centre for Polar and Marine Research, Bremerhaven, Germany

Thomas Jung

*Alfred Wegener Institute, Helmholtz Centre for Polar and Marine Research, Bremerhaven,
and University of Bremen, Bremen, Germany*

Lars Nerger

Alfred Wegener Institute, Helmholtz Centre for Polar and Marine Research, Bremerhaven, Germany

(Manuscript received 31 August 2015, in final form 14 December 2015)

ABSTRACT

The sensitivity of assimilating sea ice thickness data to uncertainty in atmospheric forcing fields is examined using ensemble-based data assimilation experiments with the Massachusetts Institute of Technology General Circulation Model (MITgcm) in the Arctic Ocean during November 2011–January 2012 and the Met Office (UKMO) ensemble atmospheric forecasts. The assimilation system is based on a local singular evolutive interpolated Kalman (LSEIK) filter. It combines sea ice thickness data derived from the European Space Agency's (ESA) Soil Moisture Ocean Salinity (SMOS) satellite and Special Sensor Microwave Imager/Sounder (SSMIS) sea ice concentration data with the numerical model. The effect of representing atmospheric uncertainty implicit in the ensemble forcing is assessed by three different assimilation experiments. The first two experiments use a single deterministic forcing dataset and a different forgetting factor to inflate the ensemble spread. The third experiment uses 23 members of the UKMO atmospheric ensemble prediction system. It avoids additional ensemble inflation and is hence easier to implement. As expected, the model-data misfits are substantially reduced in all three experiments, but with the ensemble forcing the errors in the forecasts of sea ice concentration and thickness are smaller compared to the experiments with deterministic forcing. This is most likely because the ensemble forcing results in a more plausible spread of the model state ensemble, which represents model uncertainty and produces a better forecast.

1. Introduction

Arctic sea ice is an important component of the local and global climate system. The rapid decline in extent and thickness in the last 10 years is also an important factor for Arctic shipping and marine operations. Accurate numerical prediction of sea ice has already become an urgent need (Eicken 2013). However, large uncertainties still exist in the modeled Arctic sea ice thickness and volume (Schweiger et al. 2011). To reduce uncertainties in sea ice–ocean state estimation and forecasts, the obvious way is to combine available sea ice observations and coupled ice–ocean models with advanced data assimilation techniques (Lisæter et al. 2003).

In contrast to the successfully observed sea ice concentration with satellite-based passive microwave instruments (Cavalieri and Parkinson 2012; Stroeve et al. 2012), observing sea ice thickness from space is still a great challenge (Kwok and Sulsky 2010; Kaleschke et al.

Corresponding author address: Qinghua Yang, National Marine Environmental Forecasting Center, Dahuisi 8, Haidian District, Beijing 100081, China.
E-mail: yqh@nmefc.gov.cn

2012; Tian-Kunze et al. 2014). Because of the sparsely gridded sea ice thickness observations, there are very few studies with ice thickness assimilation. Lisæter et al. (2007) examined the potential for ice thickness assimilation in coupled sea ice–ocean models with an ensemble Kalman filter (EnKF). Yang et al. (2014) assimilated the first near-real-time European Space Agency's (ESA) Soil Moisture Ocean Salinity (SMOS) satellite–based sea ice thickness data into a coupled sea ice–ocean model using a local ensemble-based singular evolutive interpolated Kalman (LSEIK) filter (Pham et al. 1998; Pham 2001). Their experiments illustrated that SMOS ice thickness leads to substantially improved first-year sea ice thickness. Both studies used a single set of deterministic atmospheric forcing fields and accounted for possible uncertainties in external forcing by either perturbing the surface winds (Lisæter et al. 2007) or inflating the forecast error covariance (Yang et al. 2014) with a so-called forgetting factor (Pham et al. 1998). However, the realistic flow-dependent atmospheric uncertainty has not been taken into account.

Since their introduction in the 1990s, atmospheric ensemble prediction systems (EPSs) have been under substantial development (e.g., Houtekamer et al. 1996; Molteni et al. 1996; Atger 1999; Jung and Leutbecher 2007). The availability of global EPSs from the leading operational centers through the THORPEX Interactive Grand Global Ensemble (TIGGE) (Park et al. 2008; Bougeault et al. 2010) offers an opportunity to test the sensitivity of existing assimilation systems to the atmospheric uncertainty. Recently, Yang et al. (2015) examined the impacts of ensemble forcing on LSEIK-based sea ice concentration data assimilation and prediction in summer. In their experiments the ensemble-forcing approach allowed for approximating the atmospheric model error statistics sufficiently well and outperformed the deterministic filter in the sea ice concentration analysis and forecasts. Sea ice thickness forecasts, however, were not significantly improved over the single forcing approach.

The conditions for assimilating sea ice data are different in summer and in winter. In the cold season, most of the sea ice concentration in the Arctic is near 100%, so that not only are the thermodynamic processes different, but also the impact of concentration data on sea ice thickness in the assimilation can be expected to be smaller or at least different from what is observed in summer. Also, since the SMOS data are most reliable for thin ice, the number of usable SMOS data points decreases as ice grows to be thicker in the cold season (Yang et al. 2014). In this study, we extend the work of Yang et al. (2015) to the cold season and to assimilate thickness data derived from SMOS. In contrast to Yang et al.

(2014), we now examine the effect of explicit accounting for atmospheric uncertainty. We investigate whether the positive influence of the atmospheric ensemble implementation is similar for the assimilation of SMOS ice thickness data in the cold season as for the assimilation of ice concentration data earlier in the year (Yang et al. 2015) and examine whether, and to what extent, the thickness assimilation shows a different behavior. To answer this question, an ensemble-based LSEIK filter is used, following Yang et al. (2014), to assimilate SSMIS sea ice concentration and SMOS thickness data into the Massachusetts Institute of Technology General Circulation Model (MITgcm; Marshall et al. 1997) over an autumn–winter transition period of 3 months: 1 November 2011–30 January 2012. This period is chosen because SMOS data are valid only for the cold season. The effectiveness of the ensemble forcing is analyzed by comparing the assimilation results with those from an assimilation experiment using deterministic control forcing.

2. Forecasting System

a. MITgcm sea ice–ocean model

This study uses the MITgcm sea ice–ocean model (see Losch et al. 2010) with a viscous-plastic (VP) rheology solved by line successive relaxation (LSR; Zhang and Hibler 1997). An Arctic regional configuration with open boundaries in both the Atlantic and Pacific sectors (Losch et al. 2010; Nguyen et al. 2011) is used. The horizontal model grid has an average spacing of 18 km and is locally orthogonal. The vertical resolution is highest in the upper ocean, with 28 vertical levels in the top 1000 m. The bathymetry is derived from the National Centers for Environmental Information [formerly the National Geophysical Data Center (NGDC)] 2-minute gridded elevations/bathymetry for the world (ETOPO2; Smith and Sandwell 1997). The open ocean boundaries are treated using monthly ocean boundary conditions provided by a global model configuration (Menemenlis et al. 2008). Monthly mean river runoff is based on the Arctic Runoff Data Base [ARDB; see Nguyen et al. (2011) for more details].

b. UKMO forcing data, TIGGE archive

Following Yang et al. (2015), we use atmospheric ensemble forecasts of the Met Office (UKMO; Bowler et al. 2008) available in the TIGGE archive. Each of the selected UKMO forecasts consists of one unperturbed "control" forecast and an ensemble of 23 forecasts with perturbed initial conditions around the control state. The reader is referred to Yang et al. (2015) for more details on the surface parameters used and the processing of the forcing data.

c. Sea ice observation data

Daily averaged sea ice thickness data derived from SMOS brightness temperatures are assimilated into the forecasting experiment. The SMOS-derived sea ice thickness product has been generated with an algorithm that is based on a sea ice thermodynamic model and a three-layer radiative transfer model (Kaleschke et al. 2010, 2012) that explicitly takes variations of ice temperature and ice salinity into account (Tian-Kunze et al. 2014; http://icdc.zmaw.de). The sea ice thickness data have a resolution of 12.5 km and are interpolated to the MITgcm grid. The maximum retrievable SMOS ice thickness varies from a few centimeters to about 1 m depending on ice temperature and ice salinity (Tian-Kunze et al. 2014). Following Yang et al. (2014), only thicknesses below 1.0 m, which are mainly located in the surrounding first-year sea ice area, are assimilated. The dataset also provides daily error estimates. These are used as the observation errors in the assimilation. Note that SMOS underestimates thickness when sea ice concentration is below 95% (Tian-Kunze et al. 2014), but this underestimation is not included in the provided error estimates, as this influence is still very uncertain (X. Tian-Kunze 2015, personal communication). In the cold season, however, the sea ice concentration in most of the Arctic Ocean is close to 100%, so we have not considered this systematic error in this study. It is worth mentioning that assumed statistics of the sea ice thickness affect the analysis of the ice conditions when combining the observations with model prediction. Prior to using the provided thickness uncertainties, which has been also done in our previous study (Yang et al. 2014), we conducted a series of sensitivity experiments. In these experiments, the thickness standard error of different values was considered spatially constant or spatially variable based on relative estimates depending on the thickness itself. The last approach had already demonstrated encouraging results. The system's prediction skills, nevertheless, had been further improved with the use of the uncertainties provided with SMOS thickness data.

Additionally, to the SMOS-derived sea ice thickness data, observations of sea ice concentration are assimilated. These observations are derived from DMSP *F17* SSMIS passive microwave data, processed by the NSIDC with the NASA team algorithm (Cavalieri and Parkinson 2012; Cavalieri et al. 1996), and interpolated to the model grid.

The system performance is assessed with different observational data. For concentration, data from European Organisation for the Exploitation of Meteorological Satellites (EUMETSAT) Ocean and Sea Ice Satellite Application Facility (OSISAF) (Eastwood et al. 2011;

http://www.osi-saf.org)—in particular, the near-real-time OSISAF data provided on a 10-km polar stereographic grid—are used. Note that the OSISAF concentration product for this period is derived from a different passive microwave sensor, SSM/I, on board a different satellite, DMSP *F15*, and processed with a different algorithm than the assimilated concentration data. Strictly speaking, these differences do not make the OSISAF and NSIDC products independent data because both are derived from passive microwave instruments, but we may assume that they are sufficiently different to be treated as independent.

Independent ice thickness observations are provided by measurements of sea ice draft from Beaufort Gyre Exploration Project (BGEP) upward-looking sonar (ULS) moorings located in the Beaufort Sea (http://www.whoi.edu/beaufortgyre) and sea ice thickness data obtained from autonomous ice mass balance (IMB) buoys (Perovich et al. 2013). The error in ULS measurements of ice draft is estimated as 0.1 m (Melling et al. 1995). Drafts are converted to thickness by multiplying by a factor of 1.1 (Nguyen et al. 2011). The accuracy of the IMB sounders is 5 mm (Richter-Menge et al. 2006). The reader is referred to Fig. 1 in Yang et al. (2014) for the location of the moorings BGEP_2011A, BGEP_2011B, and BGEP_2011D, and the tracks of the ice mass balance buoys IMB_2011K.

d. Data assimilation

The data assimilation is performed with the ensemble-based SEIK filter (Pham 2001). In analogy to the implementation used by Yang et al. (2014, 2015), the filter method is coded within the Parallel Data Assimilation Framework (PDAF; Nerger and Hiller 2013; http://pdaf.awi.de). In the SEIK filter an ensemble of model states **x** represents the state estimate (as ensemble mean) and the error estimate (the ensemble covariance matrix **P**) of this state. The data assimilation is performed by alternating forecast phases in which the model propagates the ensemble and error covariance in time, $\mathbf{x}_k^f$ and $\mathbf{P}_k^f$, respectively, and analysis steps at time k in which the model states are updated with current observations $\mathbf{y}_k$,

$$\mathbf{x}_k^a = \mathbf{x}_k^f + \mathbf{K}_k(\mathbf{y}_k - \mathbf{H}_k\mathbf{x}_k^f),$$
$$\mathbf{K}_k = \mathbf{P}_k^f\mathbf{H}_k^{\mathrm{T}}(\mathbf{H}_k\mathbf{P}_k^f\mathbf{H}_k^{\mathrm{T}} + \mathbf{R}_k)^{-1}.$$

Here a and f denote analysis and forecast, respectively. Term **K** is the so-called Kalman gain. Term **H** is the observational operator, which computes the model counterpart of the observations. Term **R** is the observational error covariance matrix. With the SEIK filter as a reduced-rank square root approach, the updated

ensemble $\mathbf{x}_k^a$ samples the analyzed model uncertainties according to leading empirical orthogonal functions (EOFs), which allows for approximating the updated model error statistics $\mathbf{P}_k^a$ with a minimum ensemble size.

The SEIK analysis applies a localization by assimilating the observational information only within a radius of 126 km (~7 grid points) around a surface grid point. Within the radius, the observations are weighted with a quasi-Gaussian weight function (Gaspari and Cohn 1999) of the distance from the analyzed grid point (see Janjić et al. 2011). To stabilize the assimilation process, a forgetting factor (Pham et al. 1998) can be applied that inflates the forecast error covariance matrix to increase the model uncertainty and to avoid a too-small ensemble spread. The covariance matrix is implicitly multiplied by the inverse of the forgetting factor. Hence, the background (and previously assimilated data) is downweighted with respect to new data by the forgetting factor. For more details on the local SEIK filter and its implementation, the reader is referred to Nerger et al. (2006), Janjić et al. (2011), Losa et al. (2012), and Yang et al. (2014).

The variability of a MITgcm integration driven by the 24-h UKMO control forecasts over the period from October to December 2011 is used to generate the initial ensemble. The trajectory of daily snapshots of the sea ice concentration and thickness simulation is decomposed into EOFs. The ensemble states are then obtained by multiplying the leading EOFs with a random matrix that preserves the standard deviation in the set of EOFs and ensures that the mean of the resulting vectors is zero (second-order exact sampling; Pham 2001). The ensemble mean is defined by adding the model state from a model run without assimilation. This study uses 23 ensemble states to match with the ensemble size of the UKMO perturbed forcing. In the forecast phase of the SEIK filter, all ensemble states are dynamically integrated with the nonlinear sea ice–ocean model driven by atmospheric forcing. Every 24 h, the analysis step combines the predicted model state with the observational information. This analysis step computes a corrected state of sea ice concentration and thickness and updates the state error covariance matrix that has been estimated from the ensemble of model states. If used, the aforementioned inflation with the forgetting factor allows one to account for possible errors in the forcing and inner model parameterizations.

e. Experiment design

The data assimilation behavior is assessed in assimilation experiments in which the LSEIK filter is applied every day over the period of 1 November 2011– 30 January 2012. For the assessment the model states after each 24-h forecast are examined.
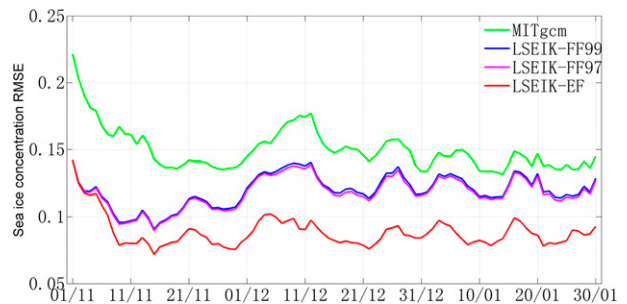

FIG. 1. Temporal evolution of RMSE differences between the independent OSISAF ice concentration data and MITgcm forecast (green solid), LSEIK-FF99 24-h forecast (blue solid), LSEIK-FF97 24-h forecast (magenta solid), and LSEIK-EF 24-h forecast (red solid) over the period 1 Nov 2011–30 Jan 2012.

Three assimilation experiments are performed. They differ only in the used atmospheric forcing and the application of the forgetting factor:

1) LSEIK-FF99: The forecasts are initialized from analyses obtained by assimilating daily NSIDC SSMIS sea ice concentration and SMOS ice thickness data and using the UKMO atmospheric control forecasts as forcing. A forgetting factor of 0.99 is applied to inflate the ensemble spread by 1%.
2) LSEIK-FF97: Similar to LSEIK-FF99, except a forgetting factor of 0.97 is applied to inflate the ensemble spread by 3%.
3) LSEIK-EF: Similar to LSEIK-FF99 and LSEIK-FF97, except the UKMO atmospheric ensemble forecasts are used as the forcing during the forecast phases. The forgetting factor was set to 1. Thus, no ensemble inflation is applied.

3. Results

a. Sea ice concentration

Figure 1 shows the temporal evolution of the root-mean-square error (RMSE) of ice concentration forecasts over the simulation period November 2011–January 2012 for the three assimilation experiments and a model forecast without data assimilation. The RMSEs are computed with respect to the independent OSISAF concentrations. Following Lisæter et al. (2003) and Yang et al. (2014), the RMSEs are computed only at grid points where either the model or the observations have ice concentrations larger than 0.05.

The data assimilation substantially reduces the deviations of the modeled sea ice concentration from the satellite-based concentrations compared to the MITgcm forecast without assimilation. Averaged over the 3-month simulation period, the mean RMSE reduces

from 0.15 for MITgcm without data assimilation (DA) to 0.12 in both LSEIK-FF99 and LSEIK-FF97, and 0.09 in LSEIK-EF. During the entire study period, the LSEIK-FF99 and LSEIK-FF97 concentrations are very similar, while the LSEIK-EF is closer to the OSISAF observations than both LSEIK-FF99 and LSEIK-FF97 concentrations. Hence, the influence of changing the forgetting factor on the ice concentration forecast is very small, while the impact of the assimilation is larger when the atmospheric uncertainty is explicitly taken into account by the ensemble forcing. During the simulation period, the sea ice concentration tends toward uniform values of 100% in most of the Arctic Ocean. While this situation leads to an increasing trend of the RMSE in LSEIK-FF99 and LSEIK-FF97 of about 25%–30% starting from 14 November 2014 to 30 January 2015, the RMSE in LSEIK-EF does not show any trend but varies between values of 0.08 and 0.1.

b. Sea ice thickness

The temporal evolution of the RMSE of the ice thickness forecast with respect to the assimilated SMOS ice thickness (<1.0 m) over the simulation period is shown in Fig. 2. The joint assimilation of sea ice concentration and SMOS sea ice thickness reduces the deviation from the thickness data for all three LSEIK forecasts. Similar to the RMSE in the sea ice concentration forecasts, the RMSE of the thickness grows during the simulation period. The total RMSEs of the run without data assimilation, the LSEIK-FF99, LSEIK-FF97, and LSEIK-EF 24-h forecasts, are 0.73, 0.25, 0.2, and 0.20 m, respectively. From the lowest error of 0.17 m, the LSEIK-FF99 error approximately doubles until the end of the experiment. However, the LSEIK-FF99 RMSE remains to be significantly lower than in the MITgcm forecast without DA. With a larger artificially inflated spread, the LSEIK-FF97 thickness is a little closer with the SMOS observations. Using ensemble forcing, the LSEIK-EF thickness agrees better with the observations than both the LSEIK-FF99 and LSEIK-FF97 thickness. This improvement in LSEIK-EF increases from November to January and reaches about 0.1 m at the end of January 2012. Yang et al. (2014) related the increase in RMSE over time to the fact that the number of observed grid points with ice thickness below 1.0 m decreases gradually. As only these observations have a sufficiently small error to be assimilated, the number of observations in the DA decreases over time. Although the RMSE in LSEIK-EF also shows an increase over time, it is much smaller than in both LSEIK-FF99 and LSEIK-FF97 by only about 62%.
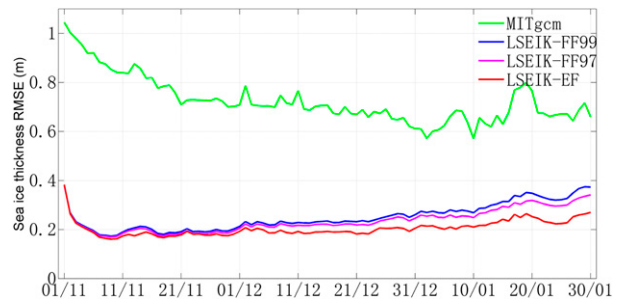

FIG. 2. Temporal evolution of RMSE differences between SMOS ice thickness (<1.0 m) and MITgcm forecast (green solid), LSEIK-FF99 24-h forecast (blue solid), LSEIK-FF97 24-h forecast (magenta solid), and LSEIK-EF 24-h forecast (red solid) over the period 1 Nov 2011–30 Jan 2012.

The spatial distributions of the mean deviation of predicted sea ice thickness from the valid SMOS data are similar for the three LSEIK experiments (Fig. 3). In particular, the LSEIK-FF99 and LSEIK-FF97 are very close to each other. However, the LSEIK-EF shows a much smaller error in most of the area with valid SMOS data, and this is consistent with the lower RMSEs shown in Fig. 2.

The comparison of the simulated ice thickness forecasts with in situ ULS and IMB buoy observations is shown in Fig. 4. All four forecasts show the gradually increasing ice thickness at BGEP_2011A, BGEP_2011B, and BGEP_2011D. Without ice thickness data assimilation, however, the model shows a bias of more than 1.0 m relative to observations. The sea ice data assimilation in all three LSEIK forecasts corrected most of the thickness bias. The RMSEs of the experiments with respect to the in situ measurements are summarized in Table 1. At BGEP_2011A and BGEP_2011D, the assimilation reduced the RMSE by 0.56–0.99 m, which is a reduction of the error by up to 79%. The improvements are smaller at BGEP_2011B, with only 0.2 m. This is caused by the fact that BGEP_2011B is closer to the central Arctic (~78°N), where the ice is thicker and in winter there are almost no SMOS observations to constrain the model by the assimilation (Yang et al. 2014). With regard to the ULS data of IMB_2011K, all four forecast solutions captured the increasing ice thickness found in the data. The three LSEIK forecasts are very close to each other and all show large improvements over the MITgcm forecast without DA. For the in situ data, the RMSEs for LSEIK-FF99, LSEIK-FF97, and LSEIK-EF in Table 1 are very similar except for BGEP_2011D, where LSEIK-EF with ensemble forcing leads to a smaller RMSE. The smaller deviation from the observations is also visible in Fig. 4c, where LSEIK-EF is closer to the
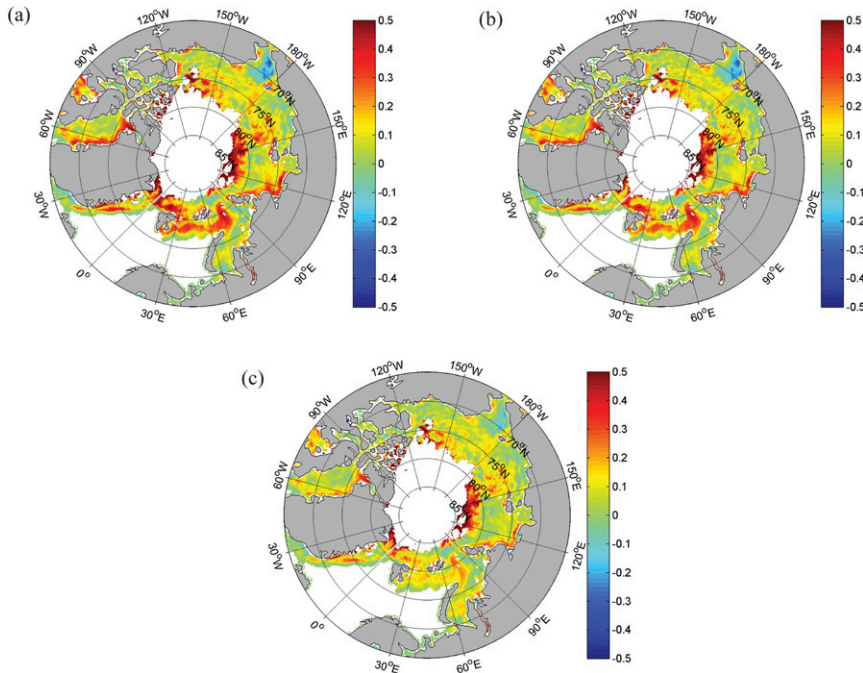
FIG. 3. Mean deviation between (a) LSEIK-FF99, (b) LSEIK-FF97, and (c) LSEIK-EF 24-h sea ice thickness forecast and the SMOS ice thickness (<1.0 m) averaged over the period 1 Nov 2011–30 Jan 2012. White shows the area of no valid SMOS observations.

data than LSEIK-FF99 and LSEIK-FF97 after 13 December. The reason for this difference will be examined in the following section.

4. Effect of the ensemble forcing

In this part we examine how the improvements of the state estimates in the three LSEIK experiments are induced. In particular, we evaluate the ensemble spread as it approximates the uncertainty in the sea ice concentration and thickness fields.

The evolution of spatially averaged sea ice concentration spread measured by the ensemble standard deviations (STDs) of the 24-h forecasts are shown in Fig. 5a. As for the RMSEs, the spread is computed only at grid points where either the modeled or observed ice
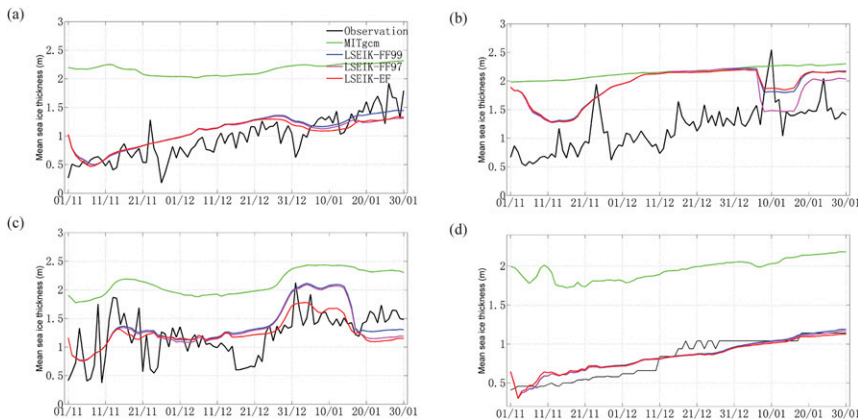

FIG. 4. Evolution of sea ice thickness (m) at (a) BGEP_2011A, (b) BGEP_2011B, (c) BGEP_2011D, and (d) IMB_2011K from 1 Nov 2011 to 30 Jan 2012. Black solid lines show the ice thickness observations. MITgcm free run, LSEIK-FF99, LSEIK-FF97, and LSEIK-EF 24-h mean ice thickness forecasts are shown as green, blue, magenta, and red solid lines, respectively.

TABLE 1. RMSE of the four forecasting experiments from in situ measurements by the ULS moorings BGEP_2011A, BGEP_2011B, and BGEP_2011D, and the IMB buoy IMB_2011K.

		BGEP_2011A	BGEP_2011B	BGEP_2011D	IMB_2011K
1	MITgcm	1.25 m	1.03 m	0.97 m	1.15 m
2	LSEIK-FF99	0.26 m	0.83 m	0.41 m	0.10 m
3	LSEIK-FF97	0.28 m	0.81 m	0.41 m	0.10 m
4	LSEIK-EF	0.27 m	0.83 m	0.35 m	0.10 m

concentrations are larger than 0.05. The initial mean STD is about 0.035 for the three LSEIK forecasts. During the assimilation experiments, the STD decreases gradually because of the assimilation of observations every 24 h and because the ice concentration tends toward uniform values of 100% in the Arctic Ocean for all members. While at the beginning the ensemble spreads of three assimilation experiments are equal, the spatially averaged spread of the LSEIK-FF97 24-h forecasts of sea ice concentration is slightly larger than LSEIK-FF99, and the LSEIK-EF is 2 times larger than both the LSEIK-FF99 and LSEIK-FF97 forecasts during the course of the experiment. Averaged over the 3-month period, the STDs are 0.005 for LSEIK-FF99, 0.006 for LSEIK-FF97, and 0.013 for LSEIK-EF. Thus, compared to LSEIK-FF99 and LSEIK-FF97, the ensemble spread of LSEIK-EF remains larger with ensemble forcing; hence, the model uncertainty is larger and allows the model ensemble to react more effectively to the observations in the analysis steps.

Figure 6 shows spatial maps of the ensemble spread (STD) of 24-h ice concentration forecasts of LSEIK-FF99, LSEIK-FF97, and LSEIK-EF for 30 January 2012. All LSEIK forecasts have their highest STDs in the sea ice edge area. Accordingly, the analysis corrections mainly occur in the sea ice edge area and the updates in the central multiyear sea ice area (with nearly 100% concentration) are very small. The STDs are a little larger for LSEIK-FF97 than for LSEIK-FF99, and are largest for LSEIK-EF. This is consistent with the mean ensemble spread shown in Fig. 5a, and it further shows that the estimated model uncertainty is largest in LSEIK-EF. The larger uncertainty estimate gives more weight to the data in the analysis step. Accordingly, LSEIK-EF provides a closer fit to concentration observations, as is visible in Fig. 1.

The evolution of spatially averaged ensemble STDs of sea ice thickness is shown in Fig. 5b. For the sea ice area with valid SMOS observations, all three LSEIK forecasts have an initial STD of about 0.09 m. Over time, the spread again decreases to about 0.02 m during a transient phase of the data assimilation of about 20 days. After this period, the STD shows a small decrease for

LSEIK-FF99 and LSEIK-FF97, although the STD for LSEIK-FF97 is a little larger than LSEIK-FF99, while the STD shows a small increase for LSEIK-EF. Averaged over the 3-month period, the STDs are 0.016 m for LSEIK-FF99, 0.019 m for LSEIK-FF97, and 0.024 m for LSEIK-EF. For the sea ice area without valid SMOS data (dotted lines in Fig. 5b), all three LSEIK forecasts have an initial STD of about 0.15 m. Over time the spread of LSEIK-FF99 and LSEIK-EF are very close to each other; both decrease to about 0.06 m after about 20 days and then fluctuate around 0.06 m. In contrast, the spread of LSEIK-FF97 increases rapidly after an initial drop and is even higher than 0.14 m by the end of January.

Figure 7 depicts the spatial distribution of the ice thickness ensemble spread on 30 January 2012 for the three LSEIK forecasts. The high STDs are mainly found in the central multiyear sea ice area, and the spread in
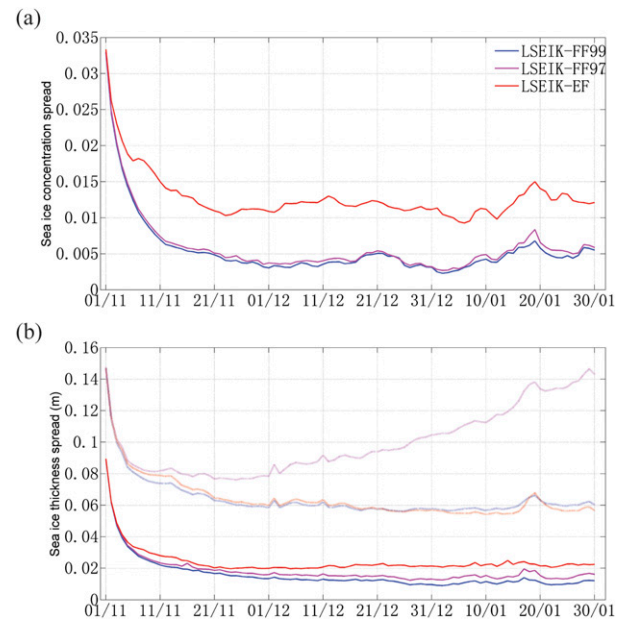

FIG. 5. Temporal evolution of area mean spread from 1 Nov 2011 to 30 Jan 2012. Spread (STDs) of LSEIK-FF99, LSEIK-FF97, and LSEIK-EF 24-h forecasts are shown as blue, magenta and red lines, respectively. (a) Ice concentration (solid lines) and (b) ice thickness forecasts over valid SMOS (0–1.0 m) area (solid lines), and ice thickness forecasts over sea ice area without valid SMOS data (dotted lines).
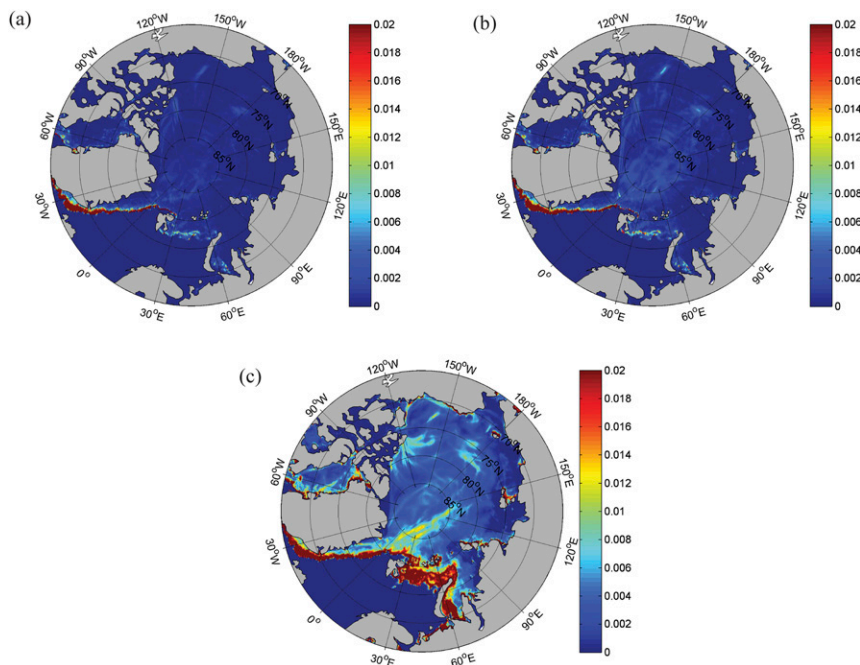
FIG. 6. Sea ice concentration STD for the individual grid cells as calculated from (a) LSEIK-FF99, (b) LSEIK-FF97, and (c) LSEIK-EF 24-h ensemble forecasts on 30 Jan 2012.

the surrounding first-year ice area is much smaller. This pattern results from the fact that the SMOS thickness data assimilation mainly influences the surrounding first-year ice area, and that it has little effect on the central thick, multiyear sea ice (that SMOS cannot detect reliably). There are notable differences between LSEIK-FF99, LSEIK-FF97, and LSEIK-EF. In particular, the spread in the central sea ice area is largest in LSEIK-FF97. The large spread in LSEIK-FF97 in this area, however, indicates that the experiment with a strong forgetting factor of 0.97 cannot constrain the ice thickness in the absence of direct thickness observations; the correlations between thickness and concentration, if present at all, are also too weak to fill the data gap. The spread in the surrounding first-year ice area is largest in LSEIK-EF (Fig. 7). The larger ensemble spread in the first-year ice area gives more weight to the SMOS ice thickness data and less weight to the model in the analysis step. Accordingly, LSEIK-EF is closer to the SMOS observations (Fig. 2). In contrast, the ensemble spread is much smaller for LSEIK-FF99; thus, the ice thickness data have a smaller influence in the data assimilation. This influence of the larger ensemble spread causes also the better estimate of the sea ice thickness at the location of BGEP_2011D visible in Fig. 4c. The spread of LSEIK-EF appears to be appropriate both in areas where there are valid SMOS data, because the model-data misfit is smallest, and in areas where there are not valid SMOS data, because the estimated model uncertainty (i.e., the

spread) is small. No uniform forgetting factor could be found to reach a similar result.

As discussed in Yang et al. (2015), the LSEIK-EF experiment with ensemble forcing is much easier to implement than the LSEIK experiment with single forcing. The forgetting factor used in LSEIK-FF99 and LSEIK-FF97 requires calibration in a series of sensitivity experiments with different values of the forgetting factor. In our application, the inflation is applied uniformly over the whole assimilation domain and for both the ice concentration and the thickness, where a different forgetting factors may have been necessary for regions with and without valid SMOS data. In this situation, the attempt to increase the inflation to improve the model-data misfit in the area of thin ice leads to the unrealistically growing ensemble spread in the area of the multiyear sea ice thickness as found in LSEIK-FF97 (Fig. 5b).

5. Summary and conclusions

In taking Yang et al. (2015) further, UKMO ensemble atmospheric forecasts of the TIGGE archive is used to simulate atmospheric uncertainty in the ensemble forecasts of sea ice thickness data assimilation with a LSEIK filter. While Yang et al. (2015) considered the assimilation of sea ice concentration data during summer, this study examines the assimilation of sea ice concentration and the SMOS ice thickness data in the cold season. We carry out two kinds of ensemble DA
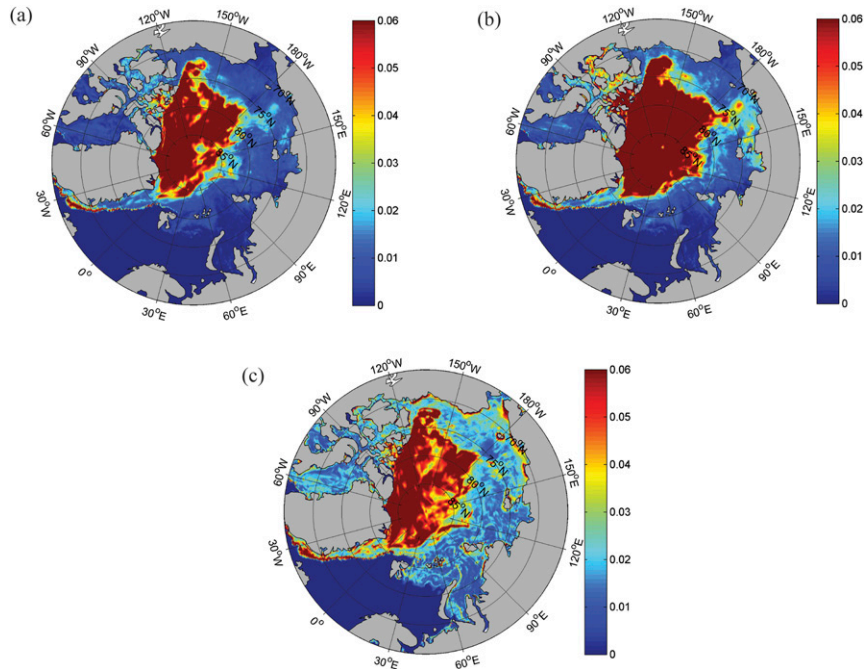
FIG. 7. Sea ice thickness STD for the individual grid cells as calculated from (a) LSEIK-FF99,
(b) LSEIK-FF97, and (c) LSEIK-EF 24-h ensemble forecasts on 30 Jan 2012.

experiments to examine the sensitivity of the results on the atmospheric forcing. The first kind (LSEIK-FF99 and LSEIK-FF97) is driven by the deterministic control forcing and uses a forgetting factor to artificially inflate the ensemble error covariance, while the second kind (LSEIK-EF) is forced by UKMO ensemble atmospheric forecasts during the data assimilation cycle. As the ensemble forcing explicitly represents atmospheric model errors, there is no need to use and tune the forgetting factor in the LSEIK-EF experiment. This simplification reduces the tuning effort and hence the configuration of the LSEIK-EF experiment is significantly easier to implement than the LSEIK-FF99 and LSEIK-FF97 experiments. With regard to the influence of using ensemble forcing, the comparisons show first that both approaches largely improve the sea ice concentration and thickness. However, both sea ice concentration and thickness forecasts based on LSEIK-EF with ensemble forcing agree better with the observation than those based on LSEIK-FF99 and LSEIK-FF97. In Yang et al. (2015), it was shown that the LSEIK-EF with ensemble forcing approach is more suitable than LSEIK-FF99 with single forcing for the sea ice concentration DA in summer. This study shows that the ensemble forcing provides a similar advantage also during the cold season and for the assimilation of sea ice thickness data.

A particular issue during the cold season is that the sea ice concentration tends toward uniform values of 100%

in the Arctic Ocean for all ensemble members (Yang et al. 2014) because of the growing sea ice in the cold season. In addition, the number of SMOS thickness observations that can be used in the assimilation decreases gradually because thickness grows beyond the range that SMOS can detect reliably. In the LSEIK-FF99 and LSEIK-FF97 experiments, this situation results in a gradual decrease of the assimilation impact on the prediction skills improvement. However, with a more realistic ensemble spread in the LSEIK-EF experiment with ensemble forcing, the error in the sea ice concentration forecasts is kept stable. Moreover, the increase of estimation errors for the sea ice thickness over the central Arctic (where there are no valid SMOS observation) pronounced in LSEIK-FF97 is significantly reduced for LSEIK-EF.

The data assimilation shows that there is considerable sensitivity to the explicit representation of forcing uncertainty by applying ensemble forcing. The forecasts and uncertainty estimates of both sea ice concentration and thickness are improved with ensemble forcing; therefore, we recommend this ensemble implementation for Arctic sea ice–ocean state estimation and real-time operational forecasts.

Finally, this study shows that the major impact of SMOS sea ice thickness data assimilation is on the surrounding first-year sea ice area, and that the improvement in the central Arctic is very small. With the

availability of near-real time *Cryosat-2* ice thickness data from April 2015 onward (http://www.cpom.ucl.ac.uk/csopr/seaice.html), it is now possible to address this issue, because *Cryosat-2* covers a thickness range (Laxon et al. 2013; Ricker et al. 2014) that is very much complementary to that of SMOS.

REFERENCES

Atger, F., 1999: The skill of ensemble prediction systems. *Mon. Wea. Rev.*, **127**, 1941–1953, doi:10.1175/1520-0493(1999)127<1941:TSOEPS>2.0.CO;2.

Bougeault, P., and Coauthors, 2010: The THORPEX Interactive Grand Global Ensemble. *Bull. Amer. Meteor. Soc.*, **91**, 1059–1072, doi:10.1175/2010BAMS2853.1.

Bowler, N. E., A. Arribas, K. R. Mylne, K. B. Robertson, and S. E. Beare, 2008: The MOGREPS short-range ensemble prediction system. *Quart. J. Roy. Meteor. Soc.*, **134**, 703–722, doi:10.1002/qj.234.

Cavalieri, D. J., and C. L. Parkinson, 2012: Arctic sea ice variability and trends, 1979–2010. *Cryosphere*, **6**, 881–889, doi:10.5194/tc-6-881-2012.

Cavalieri, D., C. Parkinson, P. Gloersen, and H. J. Zwally, 1996: Sea ice concentrations from Nimbus-7 SMMR and DMSP SSM/I-SSMIS passive microwave data, version 1 (updated yearly). NASA DAAC at the National Snow and Ice Data Center. Subset used: Sea ice concentration, accessed 12 January 2014, doi:10.5067/8GQ8LZQVL0VL.

Eastwood, S., K. R. Larsen, T. Lavergne, E. Neilsen, and R. Tonboe, 2011: Global sea ice concentration reprocessing: Product user manual. Version 1.3, EUMETSAT OSI SAF Product 0SI-409, 38 pp.

Eicken, H., 2013: Ocean science: Arctic sea ice needs better forecasts. *Nature*, **497**, 431–433, doi:10.1038/497431a.

Gaspari, G., and S. E. Cohn, 1999: Construction of correlation functions in two and three dimensions. *Quart. J. Roy. Meteor. Soc.*, **125**, 723–757, doi:10.1002/qj.49712555417.

Houtekamer, P. L., L. Lefaivre, J. Derome, H. Ritchie, and H. L. Mitchell, 1996: A system simulation approach to ensemble prediction. *Mon. Wea. Rev.*, **124**, 1225–1242, doi:10.1175/1520-0493(1996)124<1225:ASSATE>2.0.CO;2.

Janjić, T., L. Nerger, A. Albertella, J. Schröter, and S. Skachko, 2011: On domain localization in ensemble-based Kalman filter algorithms. *Mon. Wea. Rev.*, **139**, 2046–2060, doi:10.1175/2011MWR3552.1.

Jung, T., and M. Leutbecher, 2007: Performance of the ECMWF forecasting system in the Arctic during winter. *Quart. J. Roy. Meteor. Soc.*, **133**, 1327–1340, doi:10.1002/qj.99.

Kaleschke, L., N. Maaß, C. Haas, S. Hendricks, G. Heygster, and R. Tonboe, 2010: A sea-ice thickness retrieval model for 1.4 GHz radiometry and application to airborne measurements over low salinity sea-ice. *Cryosphere*, **4**, 583–592, doi:10.5194/tc-4-583-2010.

——, X. Tian-Kunze, N. Maaß, M. Mäkynen, and M. Drusch, 2012: Sea ice thickness retrieval from SMOS brightness temperatures during the Arctic freeze-up period. *Geophys. Res. Lett.*, **39**, L05501, doi:10.1029/2012GL050916.

Kwok, R., and D. Sulsky, 2010: Arctic Ocean sea ice thickness and kinematics: Satellite retrievals and modeling. *Oceanography*, **23** (4), 134–143, doi:10.5670/oceanog.2010.11.

Laxon, S. W., and Coauthors, 2013: CryoSat-2 estimates of Arctic sea ice thickness and volume. *Geophys. Res. Lett.*, **40**, 732–737, doi:10.1002/grl.50193.

Lisæter, K. A., J. Rosanova, and G. Evensen, 2003: Assimilation of ice concentration in a coupled ice–ocean model, using the Ensemble Kalman filter. *Ocean Dyn.*, **53**, 368–388, doi:10.1007/s10236-003-0049-4.

——, G. Evensen, and S. Laxon, 2007: Assimilating synthetic CryoSat sea ice thickness in a coupled ice-ocean model. *J. Geophys. Res.*, **112**, C07023, doi:10.1029/2006JC003786.

Losa, S. N., S. Danilov, J. Schröter, L. Nerger, S. Maßmann, and F. Janssen, 2012: Assimilating NOAA SST data into the BSH operational circulation model for the North and Baltic Seas: Inference about the data. *J. Mar. Syst.*, **105–108**, 152–162, doi:10.1016/j.jmarsys.2012.07.008.

Losch, M., D. Menemenlis, J.-M. Campin, P. Heimbach, and C. Hill, 2010: On the formulation of sea-ice models. Part 1: Effects of different solver implementations and parameterizations. *Ocean Modell.*, **33**, 129–144, doi:10.1016/j.ocemod.2009.12.008.

Marshall, J., A. Adcroft, C. Hill, L. Perelman, and C. Heisey, 1997: A finite-volume, incompressible Navier Stokes model for studies of the ocean on parallel computers. *J. Geophys. Res.*, **102**, 5753–5766, doi:10.1029/96JC02775.

Melling, H., P. H. Johnston, and D. A. Riedel, 1995: Measurements of the underside topography of sea ice by moored subsea sonar. *J. Atmos. Oceanic Technol.*, **12**, 589–602, doi:10.1175/1520-0426(1995)012<0589:MOTUTO>2.0.CO;2.

Menemenlis, D., J.-M. Campin, P. Heimbach, C. Hill, T. Lee, A. Nguyen, M. Schodlok, and H. Zhang, 2008: ECCO2: High resolution global ocean and sea ice data synthesis. *Mercator Ocean Quarterly Newsletter*, No. 31, Mercator Ocean, Ramonville-Saint-Agne, France, 13–21.

Molteni, F., R. Buizza, T. N. Palmer, and T. Petroliagis, 1996: The ECMWF Ensemble Prediction System: Methodology and validation. *Quart. J. Roy. Meteor. Soc.*, **122**, 73–119, doi:10.1002/qj.49712252905.

Nerger, L., and W. Hiller, 2013: Software for ensemble-based data assimilation systems—Implementation strategies and scalability. *Comput. Geosci.*, **55**, 110–118, doi:10.1016/j.cageo.2012.03.026.

——, S. Danilov, W. Hiller, and J. Schröter, 2006: Using sea-level data to constrain a finite-element primitive-equation ocean model with a local SEIK filter. *Ocean Dyn.*, **56**, 634–649, doi:10.1007/s10236-006-0083-0.

Nguyen, A. T., D. Menemenlis, and R. Kwok, 2011: Arctic ice-ocean simulation with optimized model parameters: Approach and assessment. *J. Geophys. Res.*, **116**, C04025, doi:10.1029/2010JC006573.

Park, Y.-Y., R. Buizza, and M. Leutbecher, 2008: TIGGE: Preliminary results on comparing and combining ensembles. *Quart. J. Roy. Meteor. Soc.*, **134**, 2029–2050, doi:10.1002/qj.334.

Perovich, D. K., J. A. Richter-Menge, B. Elder, T. Arbetter, K. Claffey, and C. Polashenski, 2013: Observing and understanding climate change: Monitoring the mass balance, motion, and thickness of Arctic sea ice. CRREL, accessed 14 January 2014. [Available online at http://imb.erdc.dren.mil/.]

Pham, D. T., 2001: Stochastic methods for sequential data assimilation in strongly nonlinear systems. *Mon. Wea. Rev.*, **129**, 1194–1207, doi:10.1175/1520-0493(2001)129<1194:SMFSDA>2.0.CO;2.

——, J. Verron, and L. Gourdeau, 1998: Singular evolutive Kalman filters for data assimilation in oceanography. *C. R. Acad. Sci. Ser. IIa: Sci. Terre Planetes*, **326**, 255–260, doi:10.1016/S1251-8050(97)86815-2.

Richter-Menge, J. A., D. K. Perovich, B. C. Elder, K. Claffey, I. Rigor, and M. Ortmeyer, 2006: Ice mass-balance buoys: A tool for measuring and attributing changes in the thickness of the Arctic sea-ice cover. *Ann. Glaciol.*, **44**, 205–210, doi:10.3189/172756406781811727.

Ricker, R., S. Hendricks, V. Helm, H. Skourup, and M. Davidson, 2014: Sensitivity of CryoSat-2 Arctic sea-ice freeboard and thickness on radar-waveform interpretation. *Cryosphere*, **8**, 1607–1622, doi:10.5194/tc-8-1607-2014.

Schweiger, A., R. Lindsay, J. Zhang, M. Steele, H. Stern, and R. Kwok, 2011: Uncertainty in modeled Arctic sea ice volume. *J. Geophys. Res.*, **116**, C00D06, doi:10.1029/2011JC007084.

Smith, W. H., and D. T. Sandwell, 1997: Global sea floor topography from satellite altimetry and ship depth soundings. *Science*, **277**, 1956–1962, doi:10.1126/science.277.5334.1956.

Stroeve, J. C., M. C. Serreze, N. M. Holland, J. E. Kay, J. Malanik, and A. P. Barrett, 2012: The Arctic's rapidly shrinking sea ice cover: A research synthesis. *Climatic Change*, **110**, 1005–1027, doi:10.1007/s10584-011-0101-1.

Tian-Kunze, X., L. Kaleschke, N. Maaß, M. Mäkynen, N. Serra, M. Drusch, and T. Krumpen, 2014: SMOS-derived thin sea ice thickness: Algorithm baseline, product specifications and initial verification. *Cryosphere*, **8**, 997–1018, doi:10.5194/tc-8-997-2014.

Yang, Q., S. N. Losa, M. Losch, X. Tian-Kunze, L. Nerger, J. Liu, L. Kaleschke, and Z. Zhang, 2014: Assimilating SMOS sea ice thickness into a coupled ice-ocean model using a local SEIK filter. *J. Geophys. Res. Oceans*, **119**, 6680–6692, doi:10.1002/2014JC009963.

——, ——, ——, T. Jung, and L. Nerger, 2015: The role of atmospheric uncertainty in Arctic summer sea ice data assimilation and prediction. *Quart. J. Roy. Meteor.*, **141**, 2314–2323, doi:10.1002/qj.2523.

Zhang, J., and W. Hibler III, 1997: On an efficient numerical method for modeling sea ice dynamics. *J. Geophys. Res.*, **102**, 8691–8702, doi:10.1029/96JC03744.